

doi: 10.12029/gc20190927002

甄世民,查钟健,王大钊,刘家军,庞振山,程志中,薛建玲,王江,白海军,李阳,陈超. 2023. 河北张宣地区中山沟金矿成矿流体特征及其对侵入岩型碲金矿床的限定[J]. 中国地质, 50(2): 605–621.

Zhen Shimin, Zha Zhongjian, Wang Dazhao, Liu Jiajun, Pang Zhenshan, Cheng Zhizhong, Xue Jianling, Wang Jiang, Bai Haijun, Li Yang, Chen Chao. 2023. Characteristics of ore-forming fluids of the Zhongshangou gold deposit, Zhangjiakou–Xuanhua area, Hebei Province: Limitation on the intrusive rock related telluride-gold deposits[J]. Geology in China, 50(2): 605–621(in Chinese with English abstract).

河北张宣地区中山沟金矿成矿流体特征及其对侵入岩型碲金矿床的限定

甄世民^{1,2,3},查钟健^{1,2,3},王大钊⁴,刘家军³,庞振山^{1,2},程志中^{1,2},
薛建玲^{1,2},王江³,白海军⁵,李阳⁶,陈超⁶

(1 中国地质调查局发展研究中心,北京 100037;2 自然资源部矿产勘查技术指导中心,北京 100120;3 中国地质大学地质过程与矿产资源国家重点实验室,北京 100083;4 东华理工大学核资源与环境国家重点实验室,江西 南昌 330013;5 河北省地矿局第三地质大队,河北 张家口 075000;6 河北地质大学资源学院,河北 石家庄 050031)

提要:【研究目的】中山沟金矿位于华北克拉通北缘、尚义—崇礼—赤城深大断裂的南侧,是河北省张宣金矿集区典型金矿床之一。本文探讨了矿床成矿流体特征和演化,以期为该矿床找矿勘查提供理论依据。**【研究方法】**本文总结了中山沟金矿的成矿背景、矿区地质特征、矿体及矿石特征,选取4个阶段的代表性样品,开展了流体包裹体岩相学和显微测温、氢氧同位素、氦氩同位素等研究。**【研究结果】**研究发现中山沟金矿可划分为4个成矿阶段:钾长石-黄铁矿-石英阶段(I)、乳白色石英-黄铁矿阶段(II)、烟灰色石英-硫化物阶段(III)和贫硫化物-碳酸盐阶段(IV)。各成矿阶段主要发育气液两相原生流体包裹体。流体包裹体测温数据表明,其主成矿阶段均一温度为210~250°C、盐度为6.01‰~13.62‰ NaCleqv。氢、氧同位素研究表明,δ¹⁸O_水和δD_{V-SMOW}值分别为-2.97‰~6.96‰ 和 -94.6‰~ -80.2‰,具有明显向大气降水线发生漂移而呈线性变化的特征。黄铁矿氦、氩同位素研究表明,³He/⁴He值为1.82×10⁻⁷~9.24×10⁻⁷,⁴⁰Ar/³⁶Ar值为699.9~2200.4,R/Ra值为0.13~0.66,放射成因⁴⁰Ar*为55.89%~86.57%,幔源He为2.00%~10.86%。**【结论】**中山沟金矿成矿流体经历了从中高温、中低盐度至低温、中低盐度的持续演化过程。其主成矿阶段发生了强烈的沸腾作用,成矿晚期有大量的大气降水的混入。随着成矿作用的进行,幔源物质参与成矿的比例逐渐升高。成矿流体具有壳幔混合的特点。综上所述,中山沟金矿的成矿流体具有侵入岩型碲金矿床的特点。

关 键 词:金矿;成矿流体;流体包裹体;同位素;地质调查工程;中山沟;张宣地区;河北

创 新 点:(1)总结了中山沟金矿的成矿背景、矿区地质特征、矿体及矿石特征;(2)查明了中山沟金矿流体包裹体、氢氧同位素、氦氩同位素特征;(3)厘定了中山沟金矿的成矿流体具有侵入岩型碲金矿床的特点。

中图分类号:P618.51 文献标志码:A 文章编号:1000-3657(2023)02-0605-17

Characteristics of ore-forming fluids of the Zhongshangou gold deposit, Zhangjiakou–Xuanhua area, Hebei Province: Limitation on the intrusive rock related telluride-gold deposits

收稿日期:2019-09-27;改回日期:2020-08-16

基金项目:中国地质调查局项目(DD20160052, DD20190570, DD20190159, DD20190166)及河北省自然科学基金项目(D2019403015, ZD2019003)联合资助。

作者简介:甄世民,男,1984年生,正高级工程师,从事矿床学和矿床地球化学研究;E-mail: zhenshimin0001@163.com。

ZHEN Shimin^{1,2,3}, ZHA Zhongjian^{1,2,3}, WANG Dazhao⁴, LIU Jiajun³, PANG Zhenshan^{1,2}, CHENG Zhizhong^{1,2}, XUE Jianling^{1,2}, WANG Jiang³, BAI Haijun⁵, LI Yang⁶, CHEN Chao⁶

(1. Development and Research Center of China Geological Survey, Beijing 100037, China; 2. Technical Guidance Center for Mineral Resources Exploration, Ministry of Natural Resources, Beijing 100120, China; 3. State Key Laboratory of Geological Processes and Mineral Resources, China University of Geosciences, Beijing 100083, China; 4. State Key Laboratory of Nuclear Resource and Environment, East China University of Technology, Nanchang 330013, Jiangxi, China; 5. Third Geological Brigade of Hebei Geological and Mineral Bureau, Zhangjiakou, 075000, Hebei, China; 6. College of Resources, Hebei GEO University, Shijiazhuang 050031, Hebei, China)

Abstract: This paper is the result of mineral exploration engineering.

[Objective] The Zhongshangou gold deposit is located in the north margin of North China Craton and the south side of Shangyi–Chongli–Chicheng deep fault. It is one of the typical gold deposits in Zhangjiakou–Xuanhua gold concentration area, Hebei Province. This paper discusses the characteristics and evolution of ore-forming fluids, in order to provide a theoretical basis for the exploration of the deposit. **[Methods]** This paper summarizes the regional mineralizing setting, geological characteristics of the mining area, ore body and ore characteristics. Representative samples from four metallogenic stages were selected to conduct research on fluid inclusion petrography and micro thermometry, hydrogen and oxygen isotopes, and helium and argon isotopes. **[Results]** The results indicate that it can be divided into four metallogenic stages: K-feldspar–pyrite–quartz stage (I), milky white quartz–pyrite stage (II), smoky gray quartz–sulfide stage (III) and sulfide–poor–carbonate stage (IV). Gas–liquid two-phase primary fluid inclusions are mainly developed in each mineralization stage. The temperature measurement data of fluid inclusions show that the homogenization temperature and salinity of main ore-forming stage are respectively 210–250 °C and 6.01%–13.62‰ NaCleqv. Hydrogen and oxygen isotope show that $\delta^{18}\text{O}_{\text{H}_2\text{O}}$ and $\delta\text{D}_{\text{V}-\text{SMOW}}$ values are respectively –2.97‰–6.96‰ and –94.6‰–80.2‰, which show that the $\delta^{18}\text{O}_{\text{H}_2\text{O}}$ values drift to the atmospheric water line and show a linear change. Helium and argon isotope of the pyrite show that ${}^3\text{He}/{}^4\text{He}$ values are 1.82×10^{-7} – 9.24×10^{-7} , ${}^{40}\text{Ar}/{}^{36}\text{Ar}$ values are 699.9–2200.4, R/Ra values are 0.13–0.66, radiogenic ${}^{40}\text{Ar}^*$ values are 55.89%–86.57%, and mantle derived helium values are 2.00%–10.86%. **[Conclusions]** The ore-forming fluid has experienced a continuous evolution process from medium–high temperature and medium–low salinity to low temperature and medium–low salinity. The main ore-forming stage experienced strong boiling. In the late stage of mineralization, there mixed in a large amount of meteoric water. With the development of mineralization, the proportion of mantle derived materials in mineralization increased gradually. The ore-forming fluid has the characteristics of magma fluid mixed with the crust and mantle. To sum up, the ore-forming fluid of Zhongshangou gold deposit is characterized by the intrusive rock related telluride–gold deposit.

Key words: gold deposit; ore-forming fluid; fluid inclusion; isotope; mineral exploration engineering; Zhongshangou; Zhangjiakou–Xuanhua area; Hebei Province

Highlights: (1) The regional mineralizing setting, geological characteristics of the mining area, ore body and ore characteristics are summarized; (2) The characteristics of fluid inclusion, hydrogen and oxygen isotopes, and helium and argon isotopes have been determined; (3) The ore-forming fluid of Zhongshangou gold deposit is characterized by the intrusive rock related telluride–gold deposit.

About the first author: ZHEN Shimin, male, born in 1984, senior engineer, mainly engaged in mineral deposit science and deposit geochemistry research; E-mail: zhenshimin0001@163.com.

Fund support: Supported by the projects of China Geological Survey (No.DD20160052, No.DD20190570, No.DD20190159, No. DD20190166) and Hebei Provincial Natural Science Foundation (No.D2019403015, No.ZD2019003).

1 引言

中山沟金矿位于华北克拉通北缘、尚义—崇礼

—赤城深大断裂的南侧,是张家口—宣化(简称“张宣地区”)金矿集区的典型金矿床之一。该矿床自1985年勘查发现以来,经多年找矿勘探工作,现已达

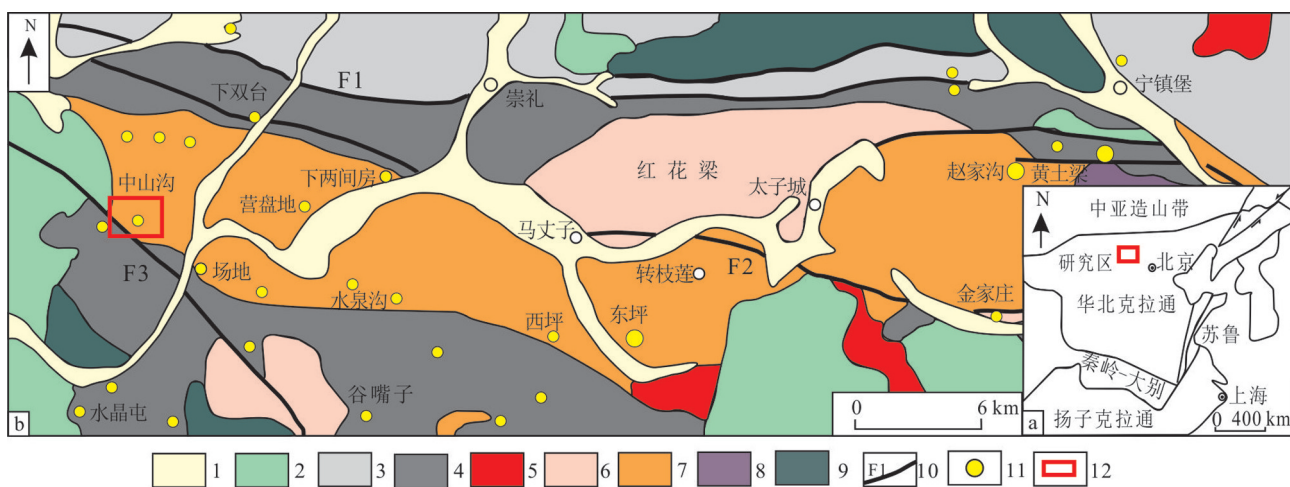


图1 大地构造位置(a)及区域地质简图(b)(据宋瑞先等, 2013; Bao et al., 2016修改)

1—第四系;2—白垩系火山岩;3—元古宇红旗营子组;4—太古宇桑干群;5—燕山期侵入岩;6—印支期侵入岩;7—海西期侵入岩;8—元古代侵入岩;9—太古宙—元古宙花岗质片麻岩;10—断层及编号;11—金矿床;12—研究区范围;F1—尚义—崇礼—赤城断裂;F2—上太子城—温泉断裂;F3—韩家沟—谷嘴子—场地断裂

Fig. 1 Sketch map of (a) geotectonic location and (b) regional geology (modified from Song Ruixian et al., 2013; Bao et al., 2016)
1—Quaternary; 2—Cretaceous volcanic rock; 3—Proterozoic Hongqiyingzi Formation; 4—Archaeozoic Sanggan Group; 5—Yanshanian intrusive rock;
6—Indosinian intrusive rock; 7—Hercynian intrusive rock; 8—Proterozoic intrusive rock; 9—Archean-Proterozoic granitic gneiss; 10—Fault and
number; 11—Gold deposit; 12—Study area; F1—Shangyi-Chongli-Chicheng fault; F2—Shangtaizicheng-Wenquan fault; F3—Hanjiagou-Guzuizi—
Changdi fault

中型矿床规模。长期以来,众多学者对中山沟金矿的成矿地质背景、矿床地质特征、矿石类型、矿物组成、控矿构造及成矿作用等进行了研究(李昌存和张增, 1999; 水兰素, 2002; Zhang et al., 2004; 邓晋福等, 2009; 吴姗姗, 2009; 郑宏伟等, 2013; 郑宏伟2014)。其中,在成矿流体方面,李昌存和韩秀丽(1998)通过流体包裹体研究,认为流体包裹体类型以气液两相为主,矿床类型为浅成中低温热液矿床;郑宏伟(2014)通过S、Pb、H、O同位素研究,认为成矿热液为原始岩浆水、变质水、大气水三者的混合热液,且成矿物质主要来自地幔。但是,近年来中山沟金矿成矿流体方面的研究工作近乎停滞,成矿流体性质、演化等方面基本为空白,严重影响了中山沟金矿的成矿机制研究,制约了找矿勘查工作。

随着新技术新方法的发展,流体包裹体、同位素联合示踪被广泛应用于示踪成矿流体。惰性气体同位素在水岩反应中基本保持不变,可以反映成矿流体来源的原始信息,尤其是He和Ar同位素已成为研究地质流体来源和多源流体混合的一种有效的方法(Simmons et al., 1987; Stuart and Turner, 1992; Stuart et al., 1994)。鉴于此,本文在系统总结前人研

究成果的基础上,通过对中山沟金矿矿床地质特征研究,结合流体包裹体岩相学、显微测温及各阶段H、O、He、Ar同位素研究,探讨了矿床成矿流体特征和演化,以期为该矿床找矿勘查提供理论依据。

2 地质背景

中山沟金矿位于河北省张宣地区,大地构造位置上处于华北克拉通北缘中段,北部与中亚造山带相邻(图1a)。张宣地区地层主要为太古宇桑干群变质岩系、吉元古界红旗营子群变质岩系、中元古界长城系、中生界白垩系和新生界第四系(宋瑞先等, 2013)。太古宇桑干群主要分布在尚义—崇礼—赤城断裂以南地区,与区内金矿的分布关系密切,其由下至上可划分为西葛峪组、水地庄组、化家营组、涧沟河组和艾家沟组,岩性主要为麻粒岩、变粒岩、片麻岩、混合岩及大理岩等,由基性—酸性火山岩变质形成。桑干群具有变质程度深、退变质作用普遍的特点(张招崇, 1995)。吉元古界红旗营子群分布在尚义—崇礼—赤城断裂以北地区,可分为底部的大同营组和顶部的庙子沟组,岩性为变粒岩、片麻岩、斜长角闪岩及大理岩等,大同营组中含

较多的石墨层。中—新元古界长城系主要出露在赤城—温泉断裂以南地区,与下伏红旗营子群为不整合接触,由下至上可划分为常州沟组、串岭沟组、团山子组、大红峪组和高于庄组(刘文建, 2014)。中生界白垩系为一套火山岩建造,主要分布在上太子城—温泉断裂(F2)以南地区。第四系冲洪积物由砂砾石、砂土及风成黄土组成。

区内构造活动频繁,断裂较发育。太古宙末期形成的尚义—崇礼—赤城断裂为本区的主要断裂构造,走向东西,全长470 km,是区内金矿最重要的控岩控矿构造。尚义—崇礼—赤城断裂在中新生代活动剧烈,大量岩浆岩沿断裂侵位,为成矿提供了有利的构造条件(图1b)。韩家沟—谷嘴子—一场地断裂走向北西—南东,长约30 km,切穿水泉沟杂岩体和张家口组火山岩(图1b)。区内褶皱构造主要发育于桑干群和红旗营子群,主要为东西向、西北向褶皱以及南北向单斜构造。区内岩浆岩具有多期次、分布广和类型丰富的特点。太古宙侵入岩主要为橄榄岩、辉长岩、闪长岩及花岗岩等,古生代岩浆岩以海西期水泉沟二长杂岩体为代表,总体呈近东西向展布,岩石类型主要为辉石闪长岩、角闪二长岩、正长岩及碱长正长岩,侵位时代为400~373 Ma,且存在自东向西年龄逐渐年轻的趋势(Miao et al., 2002; Bao et al., 2014; 李长民等, 2014)。中生代岩浆岩主要形成于三叠纪和晚侏罗世—早白垩世。三叠纪岩浆岩主要为基性—超基性岩和花岗岩,如小张家口基性—超基性岩体、红花梁二长花岗岩和谷嘴子巨斑状花岗岩等(Miao et al., 2002; Jiang et al., 2007; 田伟等, 2007; 陈茜, 2013)。晚侏罗世—早白垩世侵入岩主要为闪长岩和花岗岩,包括上水泉黑云母花岗岩、转枝莲辉石闪长岩等(Miao et al., 2002; Jiang et al., 2009; 李创举和包志伟, 2012)。区内脉岩多沿断裂发育,以海西期和燕山期为主。

目前,张宣地区已发现金矿(点)100余处,主要集中在赤城、崇礼和宣化地区,矿化样式可分为小营盘式金矿与东坪式金矿(银剑钊, 1994; 胡小蝶等, 1997; Zhen et al., 2020)。其中,东坪式金矿赋矿围岩以水泉沟二长杂岩体为特征,代表矿床为东坪、黄土梁、中山沟金矿等;小营盘式金矿赋矿围岩以桑干群变质岩为特征,代表矿床为小营盘、水晶

屯、大白阳金矿等。

3 矿床地质特征

3.1 矿区地质特征

中山沟金矿位于尚义—崇礼—赤城断裂以南和韩家沟—谷嘴子—一场地断裂以北的中间部位(图1b)。矿区出露地层较简单,仅有太古宇桑干群涧沟河组及白垩系张家口组。桑干群涧沟河组出露于矿区东南侧牧厂沟一带,岩性为斜长角闪变粒岩、斜长角闪片麻岩、斜长角闪岩及透辉角闪片麻岩等。白垩系张家口组火山岩分布于矿区西北部,不整合于水泉沟二长杂岩体之上,岩性为流纹质凝灰岩,含砾砂岩、砾岩。新生界第四系在本区分布范围较广,主要分布于河谷、山间洼地及山体的阴坡地带,厚度0~95.94 m(刘辉峰和王吉玉, 1992; 图2)。

区内构造以断裂为主,具多期活动特点。控矿构造为北北东向断裂构造,容矿构造为近南北向断裂构造。北北东向断裂主要为牧场沟断裂,倾向西,倾角50°~80°(图2),多具雁行式排列特征,表现为左旋和右旋两种,以左旋为主。断裂带常有石英脉充填,是良好的导矿构造和容矿空间(刘辉峰和王吉玉, 1992; 吴姗姗, 2009)。区内此类断裂大多分布于二长杂岩体内,成矿后的断裂活动主要继承了早期构造。

岩浆岩以海西期水泉沟二长杂岩体为主。矿区内岩体出露面积约9 km²,呈深成复合岩基产出(刘辉峰和王吉玉, 1992),岩体在牧厂沟地区与桑干群涧沟河组变质岩呈侵入接触。二长杂岩体为矿体的直接容矿围岩,与成矿作用关系密切。二长杂岩体经后期构造和热液作用形成不同类型的蚀变岩。区内脉岩受断裂控制,主要为二长岩、正长岩、钾长伟晶岩及辉绿岩等,其中以钾长伟晶岩及细晶石英二长岩最为发育。围岩蚀变主要为钾长石化、硅化、绢云母化、高岭土化及碳酸盐化等。

3.2 矿体及矿石特征

中山沟金矿主要有两条含金矿化蚀变带,即①号脉和②号脉(图3)。矿脉总体呈近南北向,倾向西,长2000余米,宽数米至数十米。其中,①号脉矿体总体呈脉状及透镜状,走向近南北,局部呈北北西及北东向,沿走向长40~280 m,倾向西,倾角50°~81°,局部变缓,倾斜延深40~270 m,厚度0.20~2.85

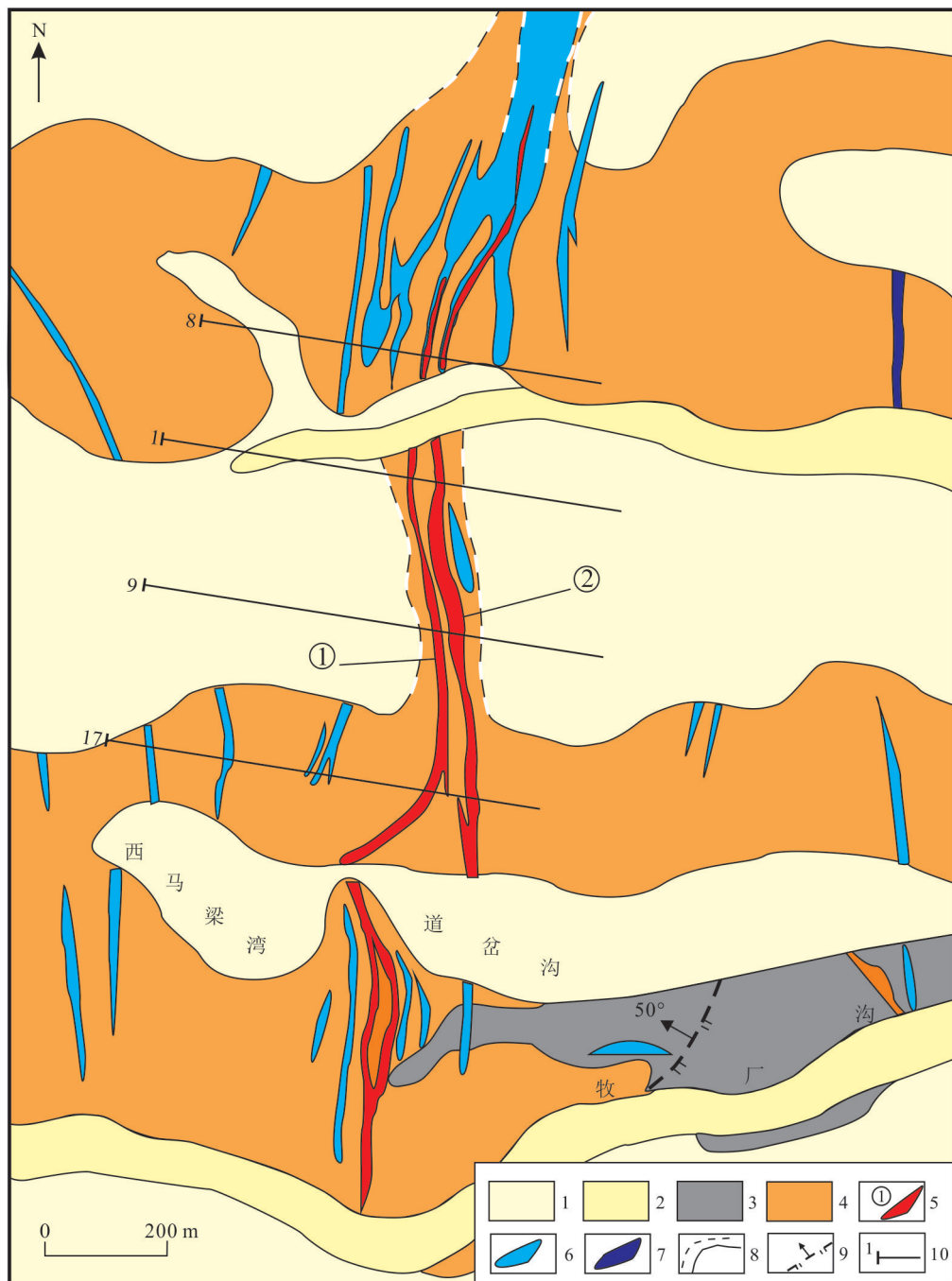


图2 中山沟金矿矿区地质图(据刘辉峰和王吉玉, 1992修编)

1—第四系全新统冲、洪积物;2—第四系上更新统冲、洪积物和风积物;3—桑干群涧沟河组;4—海西期角闪辉石二长岩;5—含金矿体的蚀变破碎带及编号;6—蚀变岩;7—断层蚀变角砾岩;8—实测(推测)地质界线;9—推断逆断层;10—勘探线位置及编号

Fig.2 Geological map of the Zhongshangou gold deposit (modified from Liu Huifeng and Wang Jiyu, 1992)

1—Holocene alluvial and diluvial sediments in the Quaternary; 2—Upper Pleistocene alluvial, diluvial and aeolian sediments in the Quaternary; 3—Metamorphic rocks of Jianggouhe Formation of Sanggan Group; 4—Hercynian hornblende pyroxene monzonite; 5—Alteration fractured zone and number of the gold-bearing orebody; 6—Altered rock; 7—Altered breccia of the fault; 8—Measured (inferred) geological boundary; 9—Presumption of reverse faults; 10—Location and number of the exploration line

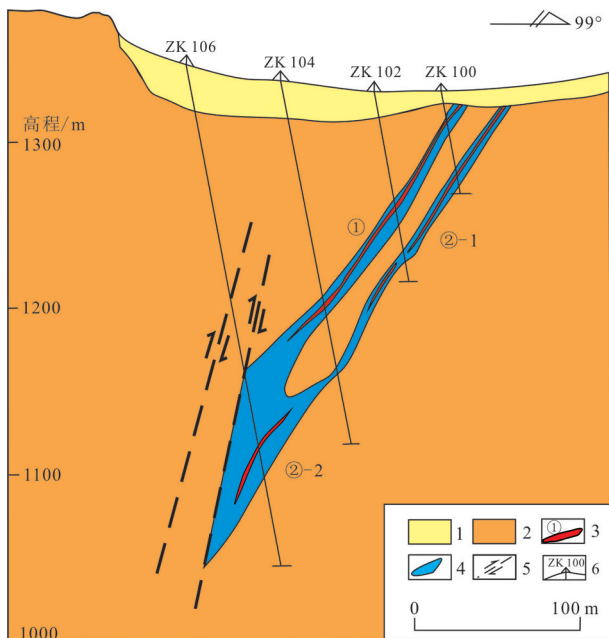


图3 中山沟金矿1号勘探线剖面图(据刘辉峰和王吉玉, 1992修编)

1—第四系;2—角闪辉石二长岩;3—含金矿体及编号;4—蚀变岩;
5—推断逆断层;6—钻孔及编号

Fig.3 Profile of No.1 geological exploration line of the Zhongshangou gold deposit (modified from Liu Huifeng and Wang Jiyu, 1992)

1—Quaternary; 2—Hercynian hornblende pyroxene monzonite; 3—Alteration fractured zone and number of the gold-bearing orebody; 4—Altered rock; 5—Inferred reverse fault; 6—Drill hole and serial numbers

m,金品位为1.60~52.57 g/t;②号脉矿体总体呈脉状及透镜状,走向近南北,局部呈北北西及北东向,沿走向长30~260 m,倾向西,倾角57°~75°,局部变缓,倾斜延伸35~215 m,厚度0.15~1.90 m,金品位为1.57~32.56 g/t(刘辉峰和王吉玉, 1992)。

矿石矿物主要为黄铁矿、方铅矿、碲金矿、闪锌矿、黄铜矿、斑铜矿、磁铁矿、赤铁矿,少量铜蓝、孔雀石、自然银、自然金、金银矿、碲铅矿和碲铋矿等(图4,图5)。脉石矿物主要为石英、钾长石、铁白云石、绢云母、重晶石、方解石及少量萤石等。矿石构造主要为稀疏浸染状构造、角砾状构造、斑杂状构造、脉状构造、块状构造、充填脉状构造及碎裂状构造等(图4a~f)。矿石结构以半自形—他形晶结构为主,其次为交代结构、交代反应边结构、他形填隙结构及不等粒压碎结构等(图4g, h, i)。

按矿石的物质成分、矿物组合和结构构造,可划分为石英脉型、钾化蚀变岩型和硅化角砾岩型3

种自然矿石类型。石英脉型矿石一般呈致密块状,局部具碎裂岩化、角砾岩化特征,主要由乳白、灰白和烟灰色石英组成(图4a),硫化物主要为黄铁矿,次为方铅矿,及少量的黄铜矿、闪锌矿和辉钼矿等,其中黄铁矿在石英中呈团斑状、团块状粗晶或呈他形细粒稠密浸染脉状分布。次生矿物主要为褐铁矿、白铅矿、孔雀石等。金矿化与黄铁矿关系密切,明金见于黄铁矿、石英晶隙及裂隙,更多见于褐铁矿中。该类型矿石的金品位一般为1~15 g/t,最高57.64 g/t,银含量2~91.4 g/t(刘辉峰和王吉玉, 1992),是最主要的矿石类型。钾化蚀变岩型矿石呈肉红色块状构造,半自形粒状和交代残余结构(图4b)。矿物成分以微斜长石为主,含量可达70%~95%,石英多呈不规则块状嵌入,或与钾长石条带相间。金属矿物主要为黄铁矿、磁铁矿及方铅矿等,呈星点状或不规则网脉状发育。该类型矿石品位比较均匀,一般为1~10 g/t,最高25.18 g/t,银可达26.3 g/t(刘辉峰和王吉玉, 1992)。该类型与含金石英脉关系密切,常发育于含金石英脉的一侧或两侧,呈带状或囊状产出,与围岩接触关系截然。硅化角砾岩型矿石呈灰色—砖红色,块状构造(图4c)。胶结物多为玉髓、石英,角砾主要为二长岩、钾化蚀变岩。角砾多呈糜棱状、碎裂状,局部见不同程度重结晶,形成变晶结构。角砾大小悬殊,大至几厘米以上,多数小于1 cm。矿石内常发育晶洞,其内发育石英晶簇、方解石及含铁碳酸盐等次生附着物。该类型矿石金品位变化大,为小于1 g/t至几十克/吨(刘辉峰和王吉玉, 1992)。

根据矿脉穿切关系、矿物共生组合等特征,可划分为4个成矿阶段(图5,图6):

(I) 钾长石—黄铁矿—石英阶段:钾化蚀变岩分布于石英脉一侧或两侧,被石英脉切穿。金属硫化物主要为黄铁矿,多呈自形—半自形—他形晶单体出现,少见其他硫化物(图5a)。

(II) 乳白色石英—黄铁矿阶段:乳白色石英脉中的硫化物以稀疏斑杂构造为主,金属矿物主要以黄铁矿为主,方铅矿次之,黄铜矿等其他硫化物少见。矿物自形程度较高,晶形较好,石英一般呈乳白色(图5b,c)。

(III) 烟灰色石英—硫化物阶段:烟灰色石英脉切割乳白色石英,黄铁矿以稠密浸染构造为特征,常富

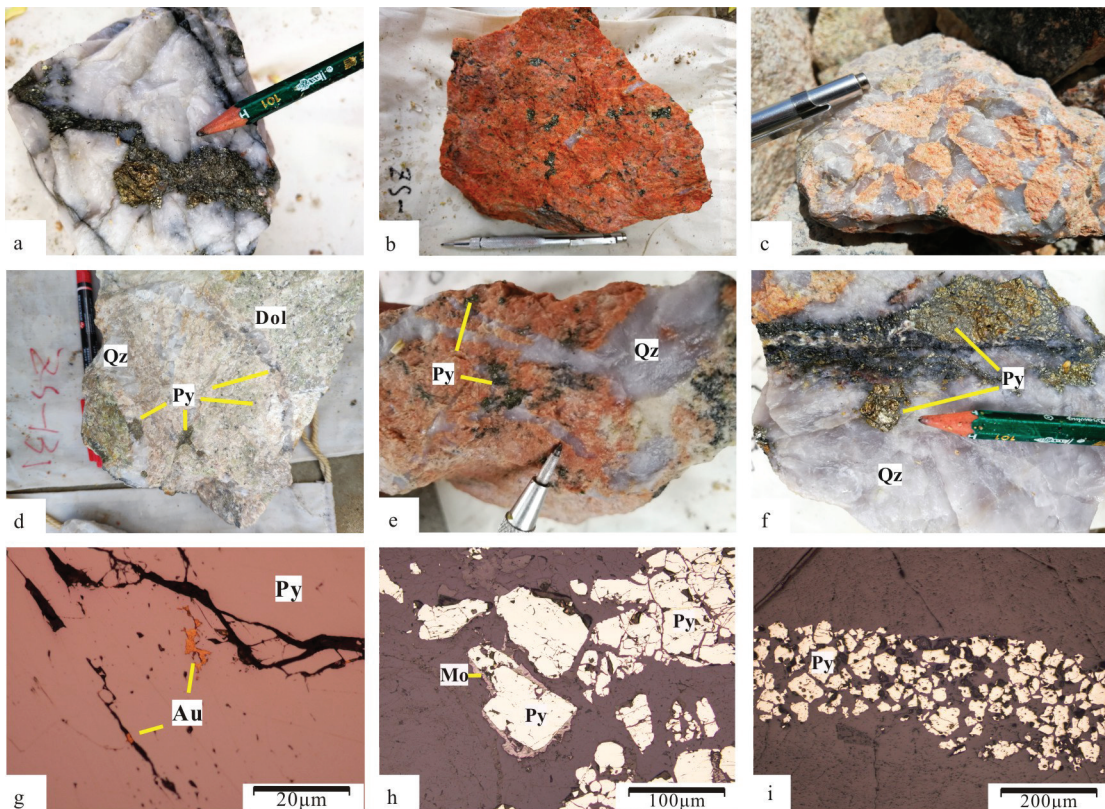


图4 中山沟金矿主要矿石类型及组构特征照片

a—石英脉型矿石;b—钾化蚀变岩型矿石;c—硅化角砾岩型矿石;d—稀疏浸染状构造;e—斑杂状构造;f—细脉状构造;g—他形填隙结构(反射光);h—交代反应边结构(反射光);i—不等粒压碎结构(反射光);Au—自然金;Dol—铁白云石;Mo—辉钼矿;Py—黄铁矿;Qz—石英
Fig.4 Photographs of the main ore types and the characteristics of ore textures and structures in the Zhongshangou gold deposit
a—Quartz vein ore; b—Potassium altered rock type ore; c—Silicified breccia ore; d—Sparse disseminated structure; e—Mottled structure; f—Veined structure; g—Heterogeneous filling structure (reflected light); h—Metasomatization reaction edge structure (reflected light); i—Unequal granular crushing structure (reflected light); Au—Natural gold; Dol—Ferrodolomite; Mo—Molybdenite; Py—Pyrite; Qz—Quartz

集成脉状或团块状集合体,自形程度低,结晶较细,辉钼矿较为发育,共生石英多呈烟灰色。此阶段金较乳白色石英阶段有明显富集,是金的主要成矿阶段,且金的富集与黄铁矿关系密切(图4g,图5d~g)。

(IV)贫硫化物-碳酸盐阶段:为热液活动的晚期产物,常叠加于硅化蚀变之后,切穿了钾化蚀变岩和石英脉。主要有方解石和含铁碳酸盐,如铁白云石等。该阶段硫化物不发育,金矿化微弱(图5h)。

4 样品采集及分析方法

在进行系统野外观察的基础上,主要在中山沟金矿的七中段、八中段及采场中采集不同成矿阶段的代表性样品。首先选择一些代表性的样品,将其磨制成厚度约0.2 mm双面抛光的包体片,然后在显微镜下对流体包裹体进行系统的观察与描述,再次对不同成矿阶段的流体包裹体进行显微测温与盐

度测试。流体包裹体的观察与显微测温和盐度测试工作是在中国地质大学(北京)流体包裹体实验室完成。测试使用Linkam THMS 600型号冷热台,温度控制范围为-196~600°C,冷冻/加热速率从0.01°C/min到130°C/min;显微测温过程中,升温速率从1~5°C/min至相变点附近降低为0.3~1°C/min。实验采用循环加热方式来测定笼合物的溶解温度,其精度范围为±0.2°C。水溶液包裹体在其冰点及某一温度附近时的升温速率一般为0.5°C/min。Linkam THMGS-600冷热台,测试精度在升温时为±1°C,降温时为±0.1°C。

同时,选取各成矿阶段的代表性样品,挑选乳白色石英-黄铁矿阶段(II)3件石英单矿物,烟灰色石英-硫化物阶段(III)6件石英单矿物和贫硫化物-碳酸盐阶段(IV)2件方解石单矿物以及9件黄铁矿单矿物。首先将含石英、方解石和黄铁矿

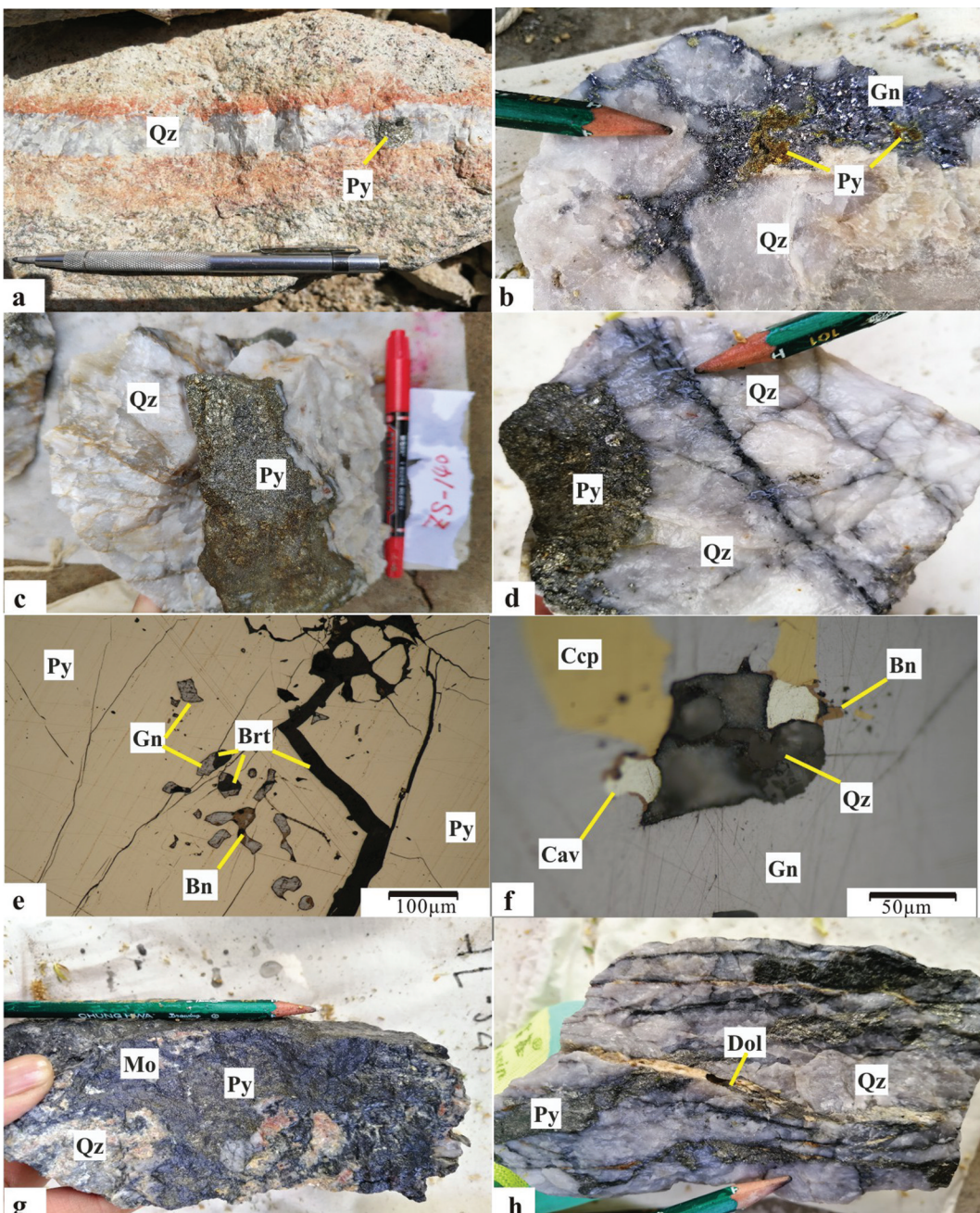


图5 中山沟金矿成矿期次与矿物组合典型照片

a—石英脉穿切钾化蚀变岩;b—乳白色石英中发育的脉状硫化物;c—乳白色石英中发育的团块状硫化物;d—烟灰色石英脉穿切乳白色石英;e—重晶石细脉穿切早期的硫化物(反射光);f—方铅矿中发育碲金矿和斑铜矿(反射光);g—烟灰色石英中发育的硫化物;h—碳酸盐脉穿切烟灰色石英脉;Bn—斑铜矿;Brt—重晶石;Cav—碲金矿;Ccp—黄铜矿;Dol—铁白云石;Gn—方铅矿;Mo—辉钼矿;Py—黄铁矿;Qz—石英

Fig.5 Typical photographs of metallogenetic stages and mineral assemblages in the Zhongshangou gold deposit

a—Quartz veins cut through the potassium altered rocks; b—Sulfide vein in the milky white quartz; c—Massive sulfide in the milky white quartz; d—Smokey grey quartz veins cut through the milky white quartz; e—Barite vein cut through the sulfide (reflected light); f—Calaverite and bornite in the galena (reflected light); g—Sulfide in the smoky grey quartz; h—Carbonate veins cut through the smoky grey quartz veins; Bn—Bornite; Brt—Barite; Cav—Calaverite; Ccp—Chalcopyrite; Dol—Ferrodolomite; Gn—Galena; Mo—Molybdenite; Py—Pyrite; Qz—Quartz

矿石样品破碎至40~80目,初步挑选出单矿物后,然后在双目显微镜下挑纯,使石英、方解石和黄铁矿单矿物的纯度大于99%,最后将挑纯的矿物送核工业北京地质研究院分析测试研究中心相关实验室进行石英、方解石的氢、氧同位素组成和黄铁矿氦氩同位素组成的分析。

石英氧同位素分析采用传统的BrF₅法,首先将研磨好的石英样品在真空条件下于500℃~680℃与纯BrF₅进行恒温反应提取矿物氧,后于700℃在铂催化剂的作用下与石墨燃烧转化成CO₂气体,最后将收集的CO₂气体进行同位素质谱测试。石英包裹体氢同位素分析采用爆裂法,首先将石英和方解石单矿物样品加热,去除矿物表面的吸附水和次生包裹体后,然后通过真空热爆法打开包裹体,分离获得H₂O,最后在真空条件下将H₂O通过锌还原法制取H₂,将收集的H₂进行质谱测试。测试采用MAT253型质谱测试,采用V-SMOW标准,氢同位素测试精度为±2‰,氧同位素测试精度为±0.2‰。

氦氩同位素的测试对象为黄铁矿单矿物。先将黄铁矿单矿物样品放置在丙酮溶液用超声波清洗20 min,然后去除杂质烘干,并在真空高温条件下去除样品表面所吸附的大气并使次生包裹体爆裂去气。再通过真空压碎法使矿物流体包裹体中释放出来的气体经4级纯化,去除活性气体,Ar,Xe被冷冻至活性碳冷阱中,纯净的He、Ne进入分析系

统,并经过加液氮的钛升华泵再次纯化,将微量的H₂、Ar去除。在-78℃的条件下释放出Ar,进入分析系统进行氩同位素分析。质谱分析采用英国产GV5400He型静态真空稀有气质谱仪,³He用电子倍增器接收,⁴He用法拉第杯接收。

5 实验结果

5.1 流体包裹体特征

5.1.1 钾长石-黄铁矿-石英阶段

该阶段流体包裹体寄主矿物为石英,主要发育气液两相原生流体包裹体,包裹体大小在3~10 μm,多数为5 μm左右,气相成分占比为15%~25%(图7a,b),多数为10%左右。该阶段类包裹体以均一至液相方式为主,测试数据8组,均一温度变化范围为300~330℃(图8a,图9)。在冷冻-升温过程中,测得该类包裹体冰点温度为-2.8~-4.3℃,依相应公式(Hall et al., 1988)计算求得相应流体盐度为4.65%~6.88% NaCl equiv(图8b)。

5.1.2 乳白色石英-黄铁矿阶段

该阶段流体包裹体寄主矿物为石英,主要发育气液两相原生流体包裹体,包裹体大小在3~10 μm,多数在5 μm左右,气相成分占比为10%~20%(图7c),多数在15%左右。此类包裹体以均一至液相方式为主,测试数据27组,均一温度变化范围为230~310℃,主要为250~290℃(图8a,图9)。在冷冻-升温过程中,测得该类包裹体冰点温度为-2.5~

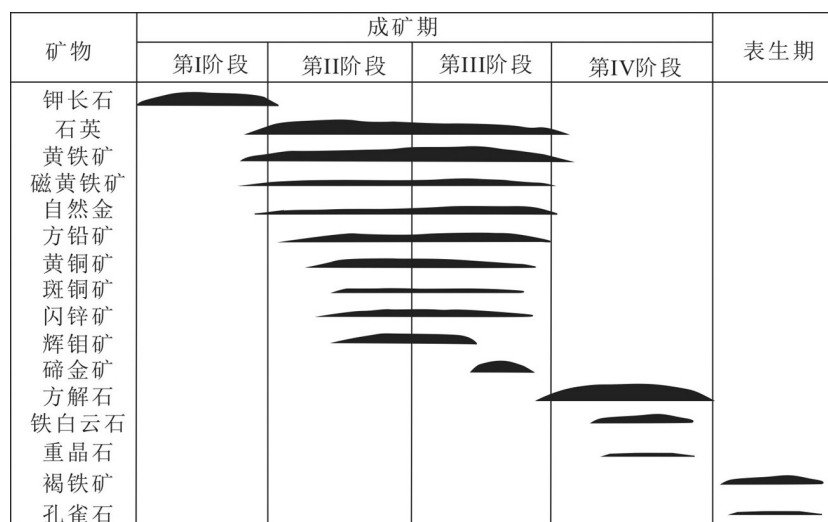


图6 中山沟金矿成矿期次与矿物生成顺序

Fig.6 Metallogenetic stages and mineral generating sequence of the Zhongshangou gold deposit

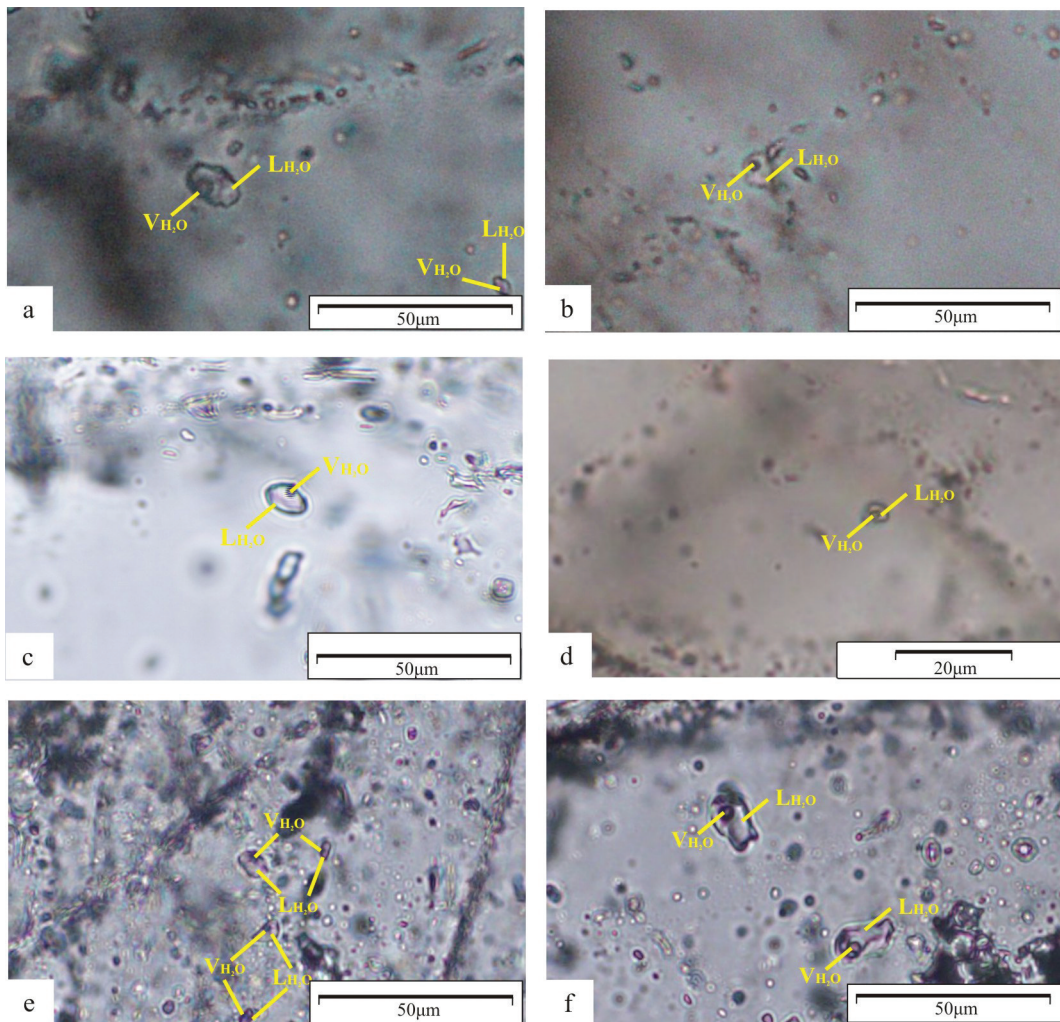


图7 石英中气液两相原生流体包裹体显微照片

Fig.7 Photomicrographs of aqueous two-phase primary fluid inclusions in the each stages quartz

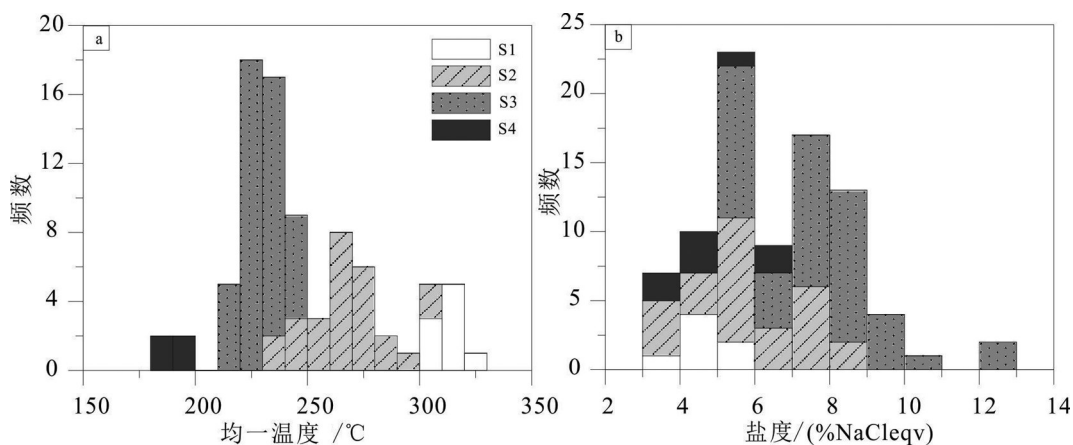


图8 流体包裹体均一温度和盐度直方图

S1—第I阶段; S2—第II阶段; S3—第III阶段; S4—第IV阶段

Fig.8 Histograms of homogeneous temperature and salinity of the fluid inclusions

S1—Stage I; S2—Stage II; S3—Stage III; S4—Stage IV

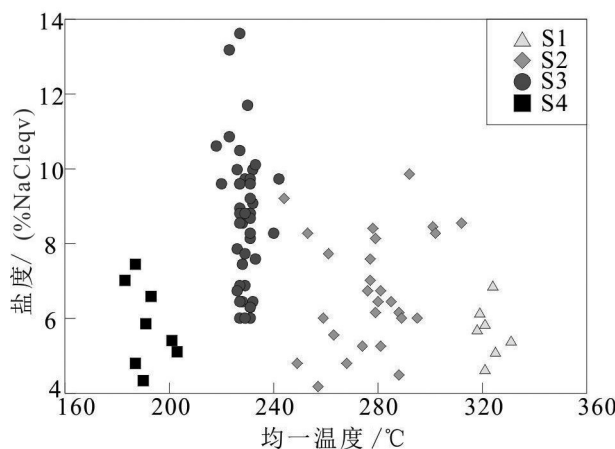


图9 流体包裹体均一温度-盐度图解

S1—第I阶段;S2—第II阶段;S3—第III阶段;S4—第IV阶段
Fig.9 Diagram showing homogeneous temperature versus salinity of the fluid inclusions

S1—Stage I; S2—Stage II; S3—Stage III; S4—Stage IV

-6.5°C, 依相应公式(Hall et al., 1988)计算求得相应流体盐度为4.18%~9.86%NaCl eqv(图8b)。

5.1.3 烟灰色石英-硫化物阶段

该阶段流体包裹体寄主矿物为石英, 主要发育气液两相原生流体包裹体, 包裹体大小在3~15 μm, 多数在5 μm左右, 气相成分占比为10%~15%(图7d), 多数在15%左右。此类包裹体以均一至液相方式为主, 测试数据47组, 均一温度变化范围

210~250°C(图8a, 图9)。在冷冻-升温过程中, 测得该类包裹体冰点温度为-3.7~-9.7°C, 依相应公式(Hall et al., 1988)求得相应流体盐度为6.01%~13.62%NaCl eqv(图8b)。

5.1.4 贫硫化物-碳酸盐阶段

该阶段流体包裹体寄主矿物为石英和方解石, 主要发育气液两相原生流体包裹体, 包裹体大小在3~10 μm, 多数在5 μm左右, 气相成分占比为10%~15%(图7e,f), 多数在10%左右。此类包裹体以均一至液相方式为主, 测试数据8组, 均一温度变化范围为180~200°C(图8a, 图9)。在冷冻-升温过程中, 测得该类包裹体冰点温度为-2.6~-4.7°C, 依相应公式(Hall et al., 1988)求得相应流体盐度为4.34%~7.45%NaCl eqv(图8b)。

5.2 氢、氧同位素特征

δD_{V-SMOW} 组成为-94.6%~-80.2%, $\delta^{18}O_{V-SMOW}$ 组成为6.4%~14%(表1)。结合对应样品的流体包裹体均一温度, 根据公式计算获得流体中 $\delta^{18}O_{H_2O}/\text{‰}$ 的值为-2.97‰~6.96‰。

5.3 氦、氩同位素特征

黄铁矿流体包裹体中的氦、氩同位素组成变化不明显。 3He 为 1.58×10^{-14} ~ $3.07 \times 10^{-13} \text{ cm}^3 \text{ STP/g}$, 4He 为 3.2×10^{-8} ~ $3.32 \times 10^{-7} \text{ cm}^3 \text{ STP/g}$, $^3He/^4He$ 为 1.82×10^{-7} ~ 9.24×10^{-7} , R/Ra为0.13~0.66, $^{40}\text{Ar}/^{36}\text{Ar}$ 含量为

表1 中山沟金矿氢、氧同位素分析结果

Table 1 Hydrogen and oxygen isotopic compositions in the Zhongshangou gold deposit

成矿阶段	测试矿物	样品编号	$\delta D_{V-SMOW}/\text{‰}$	$\delta^{18}O_{V-SMOW}/\text{‰}$	均一温度	$\delta^{18}O_{H_2O}/\text{‰}$	资料来源
第II阶段	石英	ZS-54	-87.9	11	310	3.96	本文
	石英	ZS-60	-80.2	10.4	300	3.36	
	石英	ZS-111	-90.5	14	300	6.96	
第III阶段	石英	ZS-6	-92.9	11.3	230	1.11	本文
	石英	ZS-13	-84.9	10.6	235	0.41	
	石英	ZS-34	-81.7	11.9	240	1.71	
	石英	ZS-66	-91.5	12.3	235	2.11	
	石英	ZS-67	-85.1	12.3	230	2.11	
	石英	ZS-96	-93.4	11.9	225	1.71	
第IV阶段	方解石	ZS-4	-84.4	6.4	190	-2.97	本文
	方解石	ZS-16	-91.5	6.4	190	-2.97	
吴姗姗, 2009	石英	ZS-8	-88	13.0	204	1.54	吴姗姗, 2009
	石英	ZS-13	-85	12.7	190	0.34	
	石英	ZS-19	-86.4	8.1	260	-0.4	
	石英	ZS-22	-94.6	12.88	260	4.83	

注: $\delta^{18}O_{H_2O}/\text{‰}$ 根据公式计算(Clayton et al., 1972), $1000 \ln \alpha_{\text{石英}-\text{水}} = \delta^{18}O_{\text{石英}} - \delta^{18}O_{\text{水}}$, $10^3 \ln \alpha = 3.38 \times 10^6 / T^2 - 3.4$, $1000 \ln \alpha_{\text{方解石}-\text{水}} = \delta^{18}O_{\text{方解石}} - \delta^{18}O_{\text{水}}$, $10^3 \ln \alpha = 2.78 \times 10^6 / T^2 - 2.89$ 。

699.9~2200.4(表2)。

6 讨 论

6.1 流体包裹体及氢、氧同位素的指示意义

原生包裹体可以揭示原始成矿流体的性质与来源(Fan et al., 2011; 陈衍景等, 2017; 刘嘉等, 2021)。中山沟金矿主要发育气液两相原生流体包裹体。均一温度从第I阶段超过300°C降至第IV阶段180~200°C(图8,图9)。大多数来自不同矿化阶段的流体包裹体都具有盐度<9%NaCleqv的特征。第III阶段出现高盐度(高达13.62% NaCleqv)和低盐度包裹体共存的现象,且其均一温度基本一致(图9),表明流体在第III阶段发生沸腾作用,相分离形成低盐度和高盐度两相流体。成矿流体在第IV阶段降为低盐度(图9),代表了热液系统的衰退和冷却阶段,反映了外部流体的加入,如大气降水的加入。

水是成矿流体的基本组分,形成矿床的成矿流体可能来自大气降水、海水、初生水、岩浆水、封存水(包括深成热卤水和油田水)(韩吟文和马振东,2003; 陈骏和王鹤年,2004),成矿流体的氢、氧同位素组成是区分不同来源水的重要示踪剂。中山沟金矿的 $\delta^{18}\text{O}_{\text{H}_2\text{O}}$ 值变化于-2.97‰~6.96‰, $\delta\text{D}_{\text{V-SMOW}}$ 值变化于-93.4‰~80.2‰。在 $\delta\text{D}_{\text{SMOW}}-\delta^{18}\text{O}_{\text{H}_2\text{O}}$ 图中(图10),分析结果显示投影点落在大气降水线的右侧、岩浆水的下方并偏移了岩浆水的区域范围。第II阶段到第IV阶段,流体中 $\delta^{18}\text{O}_{\text{H}_2\text{O}}$ 变化范围较大,具有明显向大气降水线发生漂移而呈线性变化的特征,反映了中山沟金矿床的成矿流体早期以岩浆水为主,伴随成矿作用

持续进行,在成矿晚期逐步混入大量的大气降水。

综上所述,中山沟金矿从钾长石-石英阶段(I)、乳白色石英-硫化物阶段(II)、烟灰色石英-硫化物阶段(III)到贫硫化物-碳酸盐阶段(IV),流体包裹体数据反映了成矿流体从中高温(300~330°C)、中低盐度(4.65%~6.88% NaCleqv)向低温(180~200°C)、中低盐度(4.34%~7.45% NaCleqv)的持续演化过程,其中主成矿阶段(III)发生了强烈的沸腾作用,氢氧同位素反映了成矿后期逐渐有大气降水的加入。流体沸腾和大气降水的混合使成矿流体的物理化学条件发生变化,从而导致硫化物、碲化物和金矿物的大量沉淀。中山沟金矿的流体包裹体类型主要为气液两相,与造山型金矿床富CO₂的包裹体不一致(Groves et al., 2020);成矿流体盐度高于浅成低温热液型金矿床(一般<5% NaCleqv; Simmons et al., 2005; Bodnar et al., 2014),成矿流体来源也与浅成低温热液金矿床(主要为大气降水; Simmons et al., 2005; Zhai et al., 2018)存在明显差异;矿体主要赋存于海西期水泉沟二长杂岩体中,成矿温度为中高温,发育大量的高温蚀变组合(如钾化),且发育大量碲化物,与张宣地区的东坪和后沟等金矿一致(Cook et al., 2009; Wang et al., 2019)。因此,中山沟金矿应属于侵入岩型碲金矿床(刘家军等,2020)。

6.2 氦、氩同位素的指示意义

矿物流体包裹体中的He除来自成矿时的热液流体外,还可能受后期扩散丢失、后生叠加及同位素分馏的影响。但前人的研究表明,当流体包裹体的寄主矿物是硫酸盐和硫化物时,包裹体内的稀有

表2 中山沟金矿黄铁矿氦、氩同位素组成

Table 2 Helium and argon isotopic compositions of pyrite in the Zhongshangou gold deposit

成矿阶段	样品号	测试矿物	^3He 含量/ 10^{-14}	^4He 含量/ 10^{-8}	$(^3\text{He}/^4\text{He})/10^{-7}$	R/Ra	$^{40}\text{Ar}/^{36}\text{Ar}$	$^{38}\text{Ar}/^{36}\text{Ar}$	幔源He占比/%	放射成因 $^{40}\text{Ar}^*$ 占比/%
第I阶段	ZS-3	黄铁矿	16.324	26.5	6.16	0.44	1908.6	0.203	7.18	84.52%
	ZS-11	黄铁矿	3.7745	6.27	6.02	0.43	952.6	0.211	7.02	68.98%
	ZS-30	黄铁矿	1.5761	8.66	1.82	0.13	898.5	0.216	2.00	67.11%
第II阶段	ZS-33	黄铁矿	2.2848	3.20	7.14	0.51	669.9	0.195	8.35	55.89%
	ZS-47	黄铁矿	14.599	15.8	9.24	0.66	1217.5	0.202	10.86	75.73%
	ZS-85	黄铁矿	7.6076	14.3	5.32	0.38	1497.6	0.196	6.18	80.27%
第III阶段	ZS-108	黄铁矿	16.695	22.5	7.42	0.53	1226.4	0.194	8.69	75.91%
	ZS-113	黄铁矿	30.677	33.2	9.24	0.66	2200.4	0.214	10.86	86.57%
	ZS-117	黄铁矿	8.1245	9.36	8.68	0.62	1419.5	0.2	10.19	79.18%

注:数据来自本次研究;同位素含量单位为cm³/g(STP);R为样品 $^3\text{He}/^4\text{He}$ 比值;Ra为大气 $^3\text{He}/^4\text{He}$ 比值,1 Ra=1.4×10⁻⁶;幔源He占比/%=[$(^3\text{He}/^4\text{He})_{\text{样品}}-(^3\text{He}/^4\text{He})_{\text{地壳}}]/[(^3\text{He}/^4\text{He})_{\text{地幔}}-(^3\text{He}/^4\text{He})_{\text{地壳}}]×100,($^3\text{He}/^4\text{He})_{\text{地壳}}$ 和($^3\text{He}/^4\text{He})_{\text{地幔}}$)的下限值分别为 $2×10^{-8}$ 和 $1.1×10^{-5}$ (Stuart et al., 1995; 徐永昌, 1996, 1998);放射成因 $^{40}\text{Ar}^*/\%=[1-295.5/(^{40}\text{Ar}/^{36}\text{Ar})_{\text{样品}}]×100$ (Kendrick et al., 2001)。$

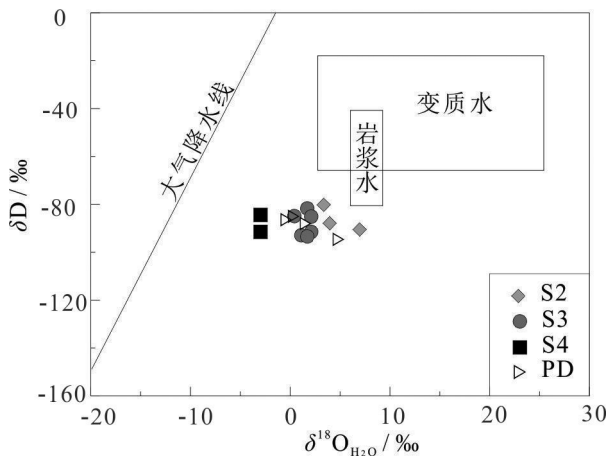


图10 中山沟金矿氢氧同位素关系图(底图据 Taylor, 1974)
S2—第II阶段;S3—第III阶段;S4—第IV阶段;PD—前人数据(据吴姗姗,2009)

Fig.10 The δD - $\delta^{18}\text{O}_{\text{H}_2\text{O}}$ composition maps of the Zhongshangou gold deposit (after Taylor, 1974)
S2—Stage II; S3—Stage III; S4—Stage IV; PD—Previous data (after Wu Shanshan, 2009)

气体被捕获后不会发生明显的扩散丢失(Trull et al., 1991; Jean-Baptiste and Fouquet, 1996; 胡瑞忠等, 1999; Hu et al., 2004)。本次测试矿物为黄铁矿,因此可以排除后期扩散丢失的影响。大量研究表明,稀有气体不同于其他稳定同位素,在流体包裹体捕获和提取过程中一般不会产生明显的同位素分馏(Podosek et al., 1981; Jean-Baptiste and Fouquet, 1996; 胡瑞忠等, 1999; Ballentine et al., 2002)。因此,本次测试的黄铁矿中流体包裹体的稀有气体组成可以代表流体的初始组成。地壳流体中稀有气体有饱和空气雨水、地幔流体和地壳放射成因三个明显不同的源区。不同来源的氦、氩同位素组成及其特征比值具有显著差别(Trull et al., 1991; Turner et al., 1993; Hu et al., 1998, 2004, 2009, 2012; Burnard et al., 1999; 张运强等, 2012; 表3)。

黄铁矿流体包裹体中的 $^3\text{He}/^4\text{He}$ 比值为0.13~0.66 Ra ($N=9$, 表2), 远低于地幔流体相应特征值(6~9 Ra), 而高于地壳流体的比值(0.01~0.05 Ra) (Stuart et al., 1995)。在 $^3\text{He}-^4\text{He}$ 图解(图11b)上, 数据测点主要落在了地壳氦与地幔氦的过渡带偏地壳组成一侧, 反映了成矿流体具有壳幔混合的特点。壳幔二元混合模式的计算结果显示(表2), 黄铁矿流体包裹体中幔源He所占比例在第I阶段为2.00%~7.18% ($N=3$), 平均值为5.40%; 第II阶段为

表3 地球中 He-Ar 来源及特征值含量
Table 3 Sources and eigenvalue of He-Ar in the earth

He-Ar 气源	$^3\text{He}/^4\text{He}$	$^{40}\text{Ar}/^{36}\text{Ar}$	$^{40}\text{Ar}/^4\text{He}$
大气饱和水 He-Ar	1 Ra	295.5	0.01
地幔流体 He-Ar	6~9 Ra	>40000	0.33~0.56
地壳放射成因 He-Ar	≤ 0.01 Ra	≥ 45000	0.16~0.25
大气 He-Ar	—	—	—

注:Ra代表大气氦的 $^3\text{He}/^4\text{He}$ 值, 为 1.4×10^{-6} 。

6.18%~10.86% ($N=3$), 平均值为8.46%; 第III阶段为8.69%~10.86% ($N=3$), 平均值为9.91%。幔源He在各阶段所占比例的不同反映了幔源物质参与成矿作用的比例逐渐升高。

$^{40}\text{Ar}/^{36}\text{Ar}$ 在第I阶段的为898.5~1908.6 ($N=3$, 表2), 平均值为1253.23; 第II阶段为669.9~1497.6 ($N=3$), 平均值为1128.33; 第III阶段为1226.4~2200.4 ($N=3$), 平均值为1615.43。这些数值远高于溶于雨水中大气氩的同位素数值($^{40}\text{Ar}/^{36}\text{Ar}=295.5$), 又大大低于地壳和地幔流体的 $^{40}\text{Ar}/^{36}\text{Ar}$ (表2, 表3)。在 $^{40}\text{Ar}/^{36}\text{Ar}-\text{R/Ra}$ 图解上(图11a), 所有样品集中分布在地壳流体和大气饱和水之间的区域, 说明流体中除了放射成因Ar外, 还有大气Ar的混入。放射成因 $^{40}\text{Ar}^*$ 含量在第I阶段67.11%~84.52% ($N=3$), 平均值为73.54% (表2); 第II阶段为55.89%~80.27% ($N=3$), 平均值为70.63%; 第III阶段为75.91%~86.57% ($N=3$), 平均值为80.55%。Qiu (1996) 和 Turner and Wang (1992)研究过流体包裹体内原地放射成因 $^{40}\text{Ar}^*$ 的产率, 结果表明, 虽然对钾或含钾矿物中的流体包裹体不能完全排除原地放射成因 $^{40}\text{Ar}^*$ 的叠加, 但对于非含钾矿物(本文属于这种情况), 其流体包裹体内原地放射成因 $^{40}\text{Ar}^*$ 的量则可忽略不计。中山沟金矿放射成因 $^{40}\text{Ar}^*$ 相对含量较高(55.89%~86.57%), 可能是由成矿流体中高含量的K衰变而来。

综上所述, $^3\text{He}/^4\text{He}$ 比值反映了成矿流体具有壳幔混合的特点。幔源He在不同成矿阶段所占比例的不同反映了幔源物质参与成矿作用的比例逐渐升高。 $^{40}\text{Ar}/^{36}\text{Ar}$ 反映了流体中除了放射成因Ar外, 还有大气Ar的混入。较高放射成因 $^{40}\text{Ar}^*$ 可能由成矿流体中高含量的K衰变而来。这些特征与河北东坪金矿(毛景文和李荫清, 2001; Mao et al., 2003)、黑龙江三道湾子金矿(余宇星等, 2012; Zhai

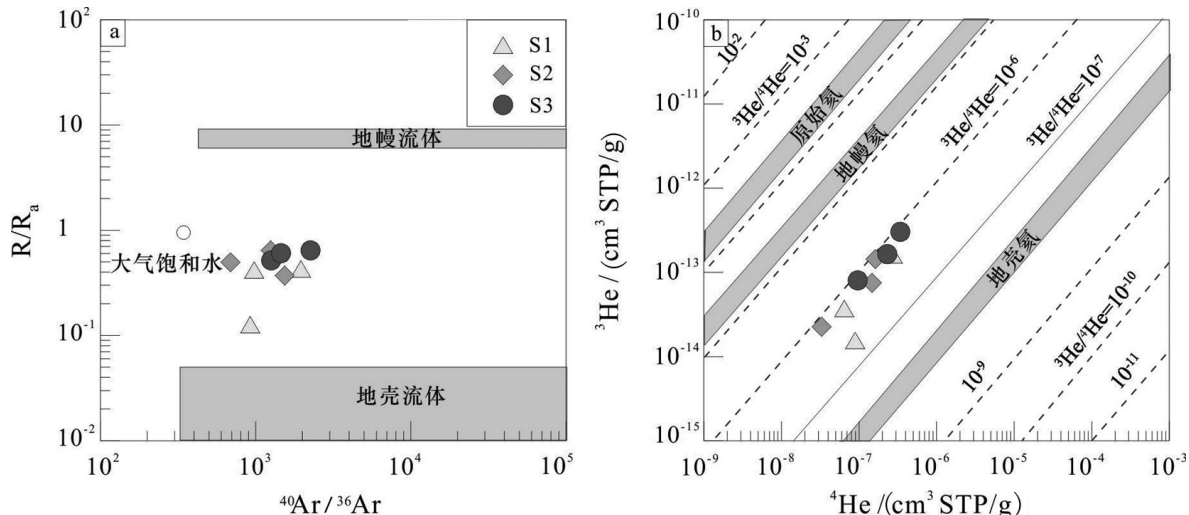


图11 中山沟金矿成矿流体 $^{40}\text{Ar}/^{36}\text{Ar}$ -R/Ra(a)和 $^{4}\text{He}-^{3}\text{He}$ 图解(b)(底图据Mamyrin and Tolstikhin, 1984修改)

S1—第I阶段; S2—第II阶段; S3—第III阶段

Fig. 11 $^{40}\text{Ar}/^{36}\text{Ar}$ -R/Ra diagram(a) and $^{4}\text{He}-^{3}\text{He}$ diagram (b) of diagram in the Zhongshangou gold deposit (modified from Mamyrin and Tolstikhin, 1984)
 S1—Stage I; S2—Stage II; S3—Stage III

et al., 2018)等富含碲化物的金矿床一致。

7 结 论

(1) 依据矿物共生组合、矿石组构及矿脉穿切关系,将中山沟金矿床划分为(I)钾长石-黄铁矿-石英、(III)乳白色石英-黄铁矿、(III)烟灰色石英-硫化物和(IV)贫硫化物-碳酸盐4个成矿阶段。其中烟灰色石英-硫化物阶段是金成矿的主要阶段。

(2) 各成矿阶段主要发育气液两相原生流体包裹体。流体包裹体测温数据表明,成矿流体经历了从中高温、中低盐度至低温、中低盐度的持续演化过程。其中主成矿阶段发生了强烈的沸腾作用,均一温度为210~250°C、盐度为6.01%~13.62% NaCl eqv。氢氧同位素反映了成矿晚期大量的大气降水的混入。

(3) 氦、氩同位素反映了成矿流体具有壳幔混合的特点。随着成矿作用的进行,幔源物质参与成矿的比例逐渐升高。高放射成因的 $^{40}\text{Ar}^*$ 可能是由成矿流体中高含量的K衰变而来。

(4) 中山沟金矿的地质特征和成矿流体特征表明其属于侵入岩型碲金矿床。

致谢:本次研究成果是一项集体成果,野外一线和室内分析人员都付出了辛勤的汗水,编写过程中得

到了多位专家的辛勤指导,在此对各位专家和项目组所有成员表示最诚挚的感谢。审稿专家在成文过程中给予了具体指导和意见,一并表示感谢。

References

- Ballentine C J, Burgess R, Marty B. 2002. Tracing fluid origin, transport and interaction in the crust[J]. Reviews in Mineralogy and Geochemistry, 47(1): 539–614.
- Bao Z W, Li C J, Zhao Z H. 2016. Metallogeny of the syenite-related Dongping gold deposit in the northern part of the North China Craton: A review and synthesis[J]. Ore Geology Reviews, 73: 198–210.
- Bao Z W, Sun W D, Li C J, Zhao Z H. 2014. U-Pb dating of hydrothermal zircon from the Dongping gold deposit in North China: Constraints on the mineralization processes[J]. Ore Geology Reviews, 61: 107–119.
- Boedner R J, Sanchez P L, Moncada D, Steele-MacInnes M. 2014. Fluid inclusions in hydrothermal ore deposits[J]. Treatise on Geochemistry, 13: 119–142.
- Burnard P G, Hu R Z, Turner G, Bi X W. 1999. Mantle, crustal and atmospheric noble gases in Ailaoshan gold deposits, Yunnan Province, China[J]. Geochimica et Cosmochimica Acta, 63(10): 1595–1604.
- Chen Jun, Wang Henian. 2004. Geochemistry[M]. Beijing: Science Press, 116–117 (in Chinese).
- Chen Qian. Studies on Fluid Characteristics and Mineralization Mechanism of the Dabaiyang Gold Deposit, Northwest of

- Hebei[D]. Beijing: China University of Geosciences (in Chinese with English abstract).
- Chen Yanjing, Ni Pei, Fan Hongrui, Pirajno F, Lai Yong, Sun Wenchao, Zhang Hui. 2007. Characteristics of fluid inclusions in different hydrothermal gold deposit systems[J]. *Acta Petrologica Sinica*, 23(9): 2085–2108 (in Chinese with English abstract).
- Clayton R N, O' Neil J R, Mayeda T K. 1972. Oxygen isotope exchange between quartz and water[J]. *Journal of Geophysical Research*, 77: 3057–3067.
- Cook N J, Ciobanu C L, Mao J W. 2009. Textural control on gold distribution in As-free pyrite from the Dongping, Huangtuliang and Houguo gold deposits, North China Craton (Hebei Province, China) [J]. *Chemical Geology*, 264(1/4): 101–121.
- Deng Jinfu, Feng Yanfang, Liu Cui, Xiao Qinghui, Su Shangguo, Zhou Su, Gao Yanguang. 2009. Yanshanian (Jurassic–Cretaceous) orogenic processes, magma sources and metallogenesis as well as coal formation in the Taihangshan–Yanshan–West Liaoning region[J]. *Geology in China*, 36 (3): 623–633 (in Chinese with English abstract).
- Fan H R, Hu F F, Wilde S A, Yang K F, Jin C W. 2011. The Qiyugou gold-bearing breccia pipes, Xiong'ershan region, central China: Fluid-inclusion and stable-isotope evidence for an origin from magmatic fluids[J]. *International Geology Review*, 53(1): 25–45.
- Groves D I, Santosh M, Zhang L. 2020. A scale-integrated exploration model for orogenic gold deposits based on a mineral system approach[J]. *Geoscience Frontiers*, 11(3): 719–738.
- Hall D L, Sternier S M, Bodnar R J. 1988. Freezing point depression of NaCl-KCl-H₂O solution[J]. *Economic Geology*, 83(1): 197–202.
- Han Yinwen, Ma Zhendong. 2003. *Geochemistry*[M]. Beijing: Geological Publishing House, 245–250 (in Chinese).
- Hu Ruizhong, Bi Xianwu, Turner G, Burnard P. 1999. He and Ar isotopic geochemistry of gold ore-forming fluids in Ailaoshan gold deposit belt[J]. *Science in China (series D)*, 29(4): 321–330 (in Chinese with English abstract).
- Hu R Z, Burnard P G, Bi X W. 2004. Helium and argon isotope geochemistry of alkaline intrusion associated gold and copper deposits along the Red River–Jinshajiang fault belt, SW China[J]. *Chemical Geology*, 203(3/4): 305–317.
- Hu R Z, Burnard P G, Bi X W, Zhou M F, Peng J T, Su W C, Zhao J H. 2009. Mantle-derived gaseous components in ore-forming fluids of the Xiangshan uranium deposit, Jiangxi Province, China: Evidence from He, Ar and C isotopes[J]. *Chemical Geology*, 266(1/2): 86–95.
- Hu R Z, Burnard P G, Turner G, Bi X W. 1998. Helium and Argon isotope systematics in fluid inclusions of Machanggong copper deposit in West Yunnan Province, China[J]. *Chemical Geology*, 146 (1/2): 55–63.
- Hu R Z, Zhou M F. 2012. Multiple Mesozoic mineralization events in South China: An introduction to the thematic issue[J]. *Mineralium Deposita*, 47(6): 579–588.
- Hu Xiaodie, Chen Zhihong, Zhao Yanming, Wang Kuiyu. 1997. The metallogenetic epoch of the Xiaoyingpan gold deposit—The new material of U-Pb isotopic age on single zircon[J]. *Progress in Precambrian Research*, 20(2): 22–28 (in Chinese with English abstract).
- Jean-Baptiste P, Fouquet Y. 1996. Abundance and isotopic composition of helium in hydrothermal sulfides from the East Pacific Rise at 13°N[J]. *Geochimica et Cosmochimica Acta*, 60(1): 87–93.
- Jiang N, Liu Y S, Zhou W G, Yang J H, Zhang S Q. 2007. Derivation of Mesozoic adakitic magmas from ancient lower crust in the North China craton[J]. *Geochimica et Cosmochimica Acta*, 71(10): 2591–2608.
- Jiang N, Zhang S Q, Zhou W G, Liu Y S. 2009. Origin of a Mesozoic granite with A-type characteristics from the North China craton: Highly fractionated from I-type magmas[J]. *Contributions to Mineralogy and Petrology*, 158: 113–130.
- Kendrick M A, Burgess R, Patrck R A D. 2001. Fluid inclusion noble gas and halogen evidence on the origin of Cu-porphyry mineralizing fluids[J]. *Geochimica et Cosmochimica Acta*, 65: 2651–2668.
- Li Changcun, Han Xiuli. 1998. Study on fluid inclusions in Zhongshan gold deposit[J]. *Gold*, 19(3): 7–9 (in Chinese with English abstract).
- Li Changcun, Zhang Zeng. 1999. The geological characteristics of Zhongshangou gold deposit[J]. *Journal of Hebei Institute of Technology*, 21: 18–21 (in Chinese with English abstract).
- Li Changmin, Deng Jinfu, Su Shangguo, Liu Cui, Liu Ximiao. 2014. U-Pb chronology and Hf isotope study of zircon in the western section of Shuiquangou rock mass, Northern Hebei Province[J]. *Acta Petrologica Sinica*, 30(11): 3301–3314 (in Chinese with English abstract).
- Li Chuangju, Bao Zhiwei. 2012. Geochemical characteristics and geodynamic implications of the Early Cretaceous magmatism in Zhangjiakou Region, northwest Hebei Province, China[J]. *Geochimica*, 41(4): 343–358 (in Chinese with English abstract).
- Liu Huirong, Wang Jiuyu. 1992. Geological Exploration Report of Zhongshangou Gold Deposit in Changdi Township, Chongli County, Hebei Province[R]. Shijiazhuang Comprehensive Geological Brigade of Hebei Bureau of Geology and Mineral Resources (in Chinese).
- Liu Jia, Cai Pengjie, Zeng Xiahua, Du Wenyan, Liu Lei. 2021. Geology, ore-forming fluid and metallogenetic age of orogenic gold deposits in the Northern Qaidam[J]. *Geology in China*, 48(2): 374–387 (in Chinese with English abstract).
- Liu Jiajun, Zhai Degao, Wang Dazhao, Gao Shen, Yin Chao, Liu Zhenjiang, Wang Jianping, Wang Yinhong, Zhang Fangfang. 2020. Classification and mineralization of the Au-(Ag)-Te-Se

- deposits[J]. *Earth Science Frontiers*, 27(2): 79–98(in Chinese with English abstract).
- Liu Wenjian. 2014. Study on Metallogenic Characteristics and Mineralization of Gold Deposits in Northern Hebei Province[D]. Beijing: China University of Geosciences (in Chinese with English abstract).
- Mamyrin B A, Tolstikhin I N. 1984. Helium isotopes in the earth's mantle[J]. *Develop Geochemical*, 3: 97–134.
- Mao J W, Li Y Q, Goldfarb R, He Y, Zaw K. 2003. Fluid inclusion and noble gas studies of the Dongping gold deposit, Hebei Province, China: A mantle connection for mineralization? [J]. *Economic Geology*, 98(3): 517–534.
- Mao Jingwen, Li Yingqing. 2001. Fluid inclusions of the Dongping gold telluride deposit in Hebei Province, China: Involvement of mantle fluid in metallogenesis[J]. *Mineral Deposits*, 20(1): 23–36(in Chinese with English abstract).
- Miao L C, Qiu Y M, Mcnaughton N, Luo Z K, Groves D, Zhai Y S, Fan W M, Zhai M G, Guan K. 2002. SHRIMP U–Pb zircon geochronology of granitoids from Dongping area, Hebei Province, China: Constraints on tectonic evolution and geodynamic setting for gold metallogeny[J]. *Ore Geology Reviews*, 19: 187–204.
- Podosek F A, Bernatowicz T J, Kramer F E. 1981. Adsorption of xenon and krypton on shales[J]. *Geochimica et Cosmochimica Acta*, 45(12): 2401–2415.
- Qiu H N. 1996. ^{40}Ar – ^{39}Ar dating of the quartz samples from two mineral deposits in western Yunnan (SW China) by crushing in vacuum[J]. *Chemical Geology*, 127: 211–222.
- Shui Lansu. 2002. Geological structural characteristics and ore control of Zhongshangou gold deposit[J]. *Journal of North China University of Technology*, 24(2): 128–131 (in Chinese with English abstract).
- Simmons S F, Sawkins F J, Schlutter D J. 1987. Mantle–derived helium in two Peruvian hydrothermal ore deposits[J]. *Nature*, 329 (6138): 429–432.
- Simmons S F, White N C, John D A. 2005. Geological characteristics of epithermal precious and base metal deposits[J]. *Economic Geology* 100th Anniversary Volume, 485–522.
- Song Ruixian, Wang Youzhi, Wang Zhenpeng. 2013. *Geological and Mineral Resources in Zhangjiakou* [M]. Beijing: Geological Publishing House, 1–188 (in Chinese).
- Stuart F M, Burnard P G, Taylor R P, Turner G. 1995. Resolving mantle and crustal contributions to ancient hydrothermal fluids: He, Ar isotopes in fluid inclusions from Dae Hwa W–Mo mineralization, South Korea[J]. *Geochimica et Cosmochimica Acta*, 59(22): 4663–4673.
- Stuart F M, Turner G. 1992. The abundance and isotopic composition of the noble gases in ancient fluids[J]. *Chemical Geology*, 101(1/2): 97–109.
- Stuart F M, Turner G, Duckworth R C, Fallick A E. 1994. Helium isotopes as tracers of trapped hydrothermal fluids in ocean–floor sulfides[J]. *Geology*, 22 (9): 823–826.
- Taylor H P. 1974. The application of oxygen and hydrogen isotope studies to problems of hydrothermal alteration and ore deposition[J]. *Economic Geology*, 69: 843–883.
- Tian Wei, Chen Bin, Liu Chaoqun, Zhang Huafeng. 2007. Zircon U–Pb age and Hf isotope composition of Xiaozhangjiakou ultra–basic rock mass in Northern Hebei Province[J]. *Acta Petrologica Sinica*, 23(3): 583–590 (in Chinese with English abstract).
- Trull T, Kurz M D, Jenkins W I. 1991. Diffusion of cosmogenic ^3He in olivine and quartz: Implications for surface exposure dating[J]. *Earth and Planetary Science Letters*, 103(1/4): 241–256.
- Turner G, Burnard P, Ford J L, Gilmour J D, Lyon I C, Stuart F M. 1993. Tracing fluid sources and interactions[J]. *Philosophical Transactions of the Royal Society of London Series A: Mathematical Physical and Engineering Sciences*, 344(1670): 127–140.
- Turner G, Wang S S. 1992. Excess argon, crustal fluid and apparent isochrons from crushing K feldspar[J]. *Earth and Planetary Science Letters*, 110: 193–211.
- Wang D Z, Liu J J, Zhai D G, Carranza E J M, Wang Y H, Zhen S M, Wang J, Wang J P, Liu Z J, Zhang F F. 2019. Mineral paragenesis and ore–forming processes of the Dongping gold deposit, Hebei Province, China[J]. *Resource Geology*, 69(3): 287–313.
- Wu Shanshan. 2009. Metallogenic and Ore–controlling Structures of Zhongshan Gold Deposit in Chongli, Hebei Province[D]. Shijiazhuang: Shijiazhuang University of Economics (in Chinese with English abstract).
- Xu Yongchang. 1996. Mantle source noble gas in natural gas[J]. *Geoscience Frontiers*, 3(3): 63–71 (in Chinese with English abstract).
- Xu Yongchang. 1998. *Rare Gas Geochemistry in Natural Gas*[M]. Beijing: Science Press, 1–104 (in Chinese).
- Yin Jianzhao. 1994. Study on the types of gold deposits in the Northwestern Hebei Province[J]. *Journal of Precious Metallic Geology*, 3(3): 176–185(in Chinese with English abstract).
- Yu Yuxing, Xu Hong, Wu Xiangke, Yang Lijun, Tian Zhu, Gao Shen, Wang Qiushu. 2012. Characteristics of the Au–Ag–Te minerals and its ore–forming fluids in Sandawanzi gold deposit, Heilongjiang Province[J]. *Acta Petrologica Sinica*, 28(1): 345–356 (in Chinese with English abstract).
- Zhai D G, Williams–Jones A E, Liu J J, Tombros S F, Cook N J. 2018. Mineralogical, fluid inclusion, and multiple isotope (H–O–S–Pb) constraints on the genesis of the Sandawanzi epithermal Au–Ag–Te deposit, NE China[J]. *Economic Geology*, 113(6): 1359–1382.
- Zhang P H, Zhu J C, Zhao Z H, Gu XP, Lin J F. 2004. Zincospiroffite, a new tellurite mineral species from the Zhongshangou gold deposit, Hebei Province, People's Republic of China[J]. *The Canadian Mineralogist*, 42: 763–768.
- Zhang Yunqiang, Li Shengrong, Chen Haiyan, Zhang Xiubao, Zhou

- Qifeng, Cui Juchao, Song Yubo, Guo Jie. 2012. Trace element and He-Ar isotopic evidence of pyrite for the source of ore-forming fluids in the Jinqingding gold deposit, eastern Shandong Province[J]. Geology in China, 39(1): 195–204 (in Chinese with English abstract).
- Zhang Zhaochong. 1995. Genesis Mechanism of Shuiquangou Complex and its Relationship with Gold Mineralization in Northern Hebei Province[D]. Beijing: Chinese Academy of Sciences (in Chinese with English abstract).
- Zhen S M, Wang Q F, Wang D Z, Emmanuel J M C, Liu J J, Pang Z S, Cheng Z Z, Xue J L, Wang J, Zha Z J. 2020. Genesis of the Zhangquanzhuang gold deposit in the northern margin of North China Craton: Constraints from deposit geology and ore isotope geochemistry[J]. Ore Geology Reviews, 122: 103511.
- Zheng Hongwei, Wang Fengxiang, Song Peng, Wang Guochen. 2013. Study on metallogenesis of Zhongshangou gold deposit[J]. Science and Technology Vision, 19: 177–177 (in Chinese with English abstract).
- Zheng Hongwei. 2014. Geological Characteristics and Genesis of the Shuijingtun Gold Deposit and Zhongshangou Gold Deposit in Zhangxuan Area[D]. Shijiazhuang: Shijiazhuang University of Economics, 1–66 (in Chinese with English abstract).

附中文参考文献

- 陈骏, 王鹤年. 2004. 地球化学[M]. 北京: 科学出版社, 116–117.
- 陈茜. 2013. 冀西北大白阳金矿成矿流体及成矿机制研究[D]. 北京: 中国地质大学.
- 陈衍景, 倪培, 范宏瑞, Pirajno F, 赖勇, 苏文超, 张辉. 2007. 不同类型热液金矿系统的流体包裹体特征[J]. 岩石学报, 23(9): 2085–2108.
- 邓晋福, 冯艳芳, 刘翠, 肖庆辉, 苏尚国, 周肃, 高延光. 2009. 太行—燕辽地区燕山期造山过程、岩浆源区与成矿作用[J]. 中国地质, 36(3): 623–633.
- 韩吟文, 马振东. 2003. 地球化学[M]. 北京: 地质出版社, 245–250.
- 胡瑞忠, 毕献武, Turner G, Bernard P. 1999. 哀牢山金矿带金成矿流体 He 和 Ar 同位素地球化学[J]. 中国科学(D辑), 29(4): 321–330.
- 胡小蝶, 陈志宏, 赵彦明, 王魁元. 1997. 河北小营盘金矿成矿时代——单颗粒锆石 U-Pb 同位素年龄新证据[J]. 前寒武纪研究进展, 20(2): 22–28.
- 李昌存, 韩秀丽. 1998. 中山沟金矿流体包裹体研究[J]. 黄金, 19(3): 7–9.
- 李昌存, 张增. 1999. 中山沟金矿床地质特征[J]. 河北联合大学学报, 21: 18–21.
- 李长民, 邓晋福, 苏尚国, 刘翠, 刘新秒. 2014. 冀北水泉沟岩体西段锆石 U-Pb 年代学及 Hf 同位素研究[J]. 岩石学报, 30(11): 3301–3314.
- 李创举, 包志伟. 2012. 冀西北早白垩世岩浆岩的地球化学特征及其地球动力学背景[J]. 地球化学, 41(4): 343–358.
- 刘辉峰, 王吉玉. 1992. 河北省崇礼县场地乡中山沟金矿勘探地质报告[R]. 河北省地质矿产局石家庄综合地质大队.
- 刘嘉, 蔡鹏捷, 曾小华, 杜文洋, 刘雷. 2021. 柴达木盆地北缘造山型金矿地质、成矿流体及成矿时代特征[J]. 中国地质, 48(2): 374–387.
- 刘家军, 翟德高, 王大钊, 高燊, 尹超, 柳振江, 王建平, 王银宏, 张方方. 2020. Au-(Ag)-Te-Se 成矿系统与成矿作用[J]. 地学前缘, 27(2): 79–98.
- 刘文建. 2014. 冀北金矿成矿特征及成矿作用研究[D]. 北京: 中国地质大学.
- 毛景文, 李荫清. 2001. 河北省东坪碲化物金矿床流体包裹体研究: 地幔流体与成矿关系[J]. 矿床地质, 20(1): 23–36.
- 水兰素. 2002. 中山沟金矿地质构造特征及控矿[J]. 华北理工大学学报, 24(2): 128–131.
- 宋瑞先, 王有志, 王振彭. 2013. 张家口地质矿产[M]. 北京: 地质出版社, 1–188.
- 田伟, 陈斌, 刘超群, 张华锋. 2007. 冀北小张家口超基性岩体的锆石 U-Pb 年龄和 Hf 同位素组成[J]. 岩石学报, 23(3): 583–590.
- 吴姗姗. 2009. 河北崇礼中山沟金矿成矿控矿构造研究[D]. 石家庄: 石家庄经济学院.
- 徐永昌. 1996. 天然气中的幔源稀有气体[J]. 地学前缘, 3(3): 63–71.
- 徐永昌. 1998. 天然气中稀有气体地球化学[M]. 北京: 科学出版社, 1–104.
- 银剑钊. 1994. 冀西北地区金矿类型研究[J]. 贵金属地质, 3(3): 176–185.
- 余宇星, 许虹, 吴祥珂, 杨利军, 田竹, 高燊, 王秋舒. 2012. 黑龙江三道湾子金矿 Au-Ag-Te 系列矿物特征及其成矿流体[J]. 岩石学报, 28(1): 345–356.
- 张运强, 李胜荣, 陈海燕, 张秀宝, 周起凤, 崔举超, 宋玉波, 郭杰. 2012. 胶东金青顶金矿床成矿流体来源的黄铁矿微量元素及 He-Ar 同位素证据[J]. 中国地质, 39(1): 195–204.
- 张招崇. 1995. 冀北水泉沟杂岩体的成因机制及其与金的成矿作用关系的研究[D]. 北京: 中国科学院.
- 郑宏伟, 王丰翔, 宋鹏, 王国晨. 2013. 中山沟金矿成矿作用研究[J]. 科技视界, 19: 177–177.
- 郑宏伟. 2014. 张宣地区水晶屯金矿和中山沟金矿地质特征对比及矿床成因探讨[D]. 石家庄: 石家庄经济学院, 1–66.